

Value of contrast-enhanced CT based radiomic machine learning algorithm in differentiating gastrointestinal stromal tumors with *KIT* exon 11 mutation: a two-center study

Bo Liu 

Hao Liu 

Lequan Zhang 

Yancheng Song 

Shifeng Yang 

Ziwen Zheng 

Junjiang Zhao 

Feng Hou 

Jian Zhang 

PURPOSE

Knowing the genetic phenotype of gastrointestinal stromal tumors (GISTs) is essential for patients who receive therapy with tyrosine kinase inhibitors. The aim of this study was to develop a radiomic algorithm for predicting GISTs with *KIT* exon 11 mutation.

METHODS

We enrolled 106 patients (80 in the training set, 26 in the validation set) with clinicopathologically confirmed GISTs from two centers. Preoperative and postoperative clinical characteristics were selected and analyzed to construct the clinical model. Arterial phase, venous phase, delayed phase, and tri-phase combined radiomics algorithms were generated from the training set based on contrast-enhanced computed tomography (CE-CT) images. Various radiomics feature selection methods were used, namely least absolute shrinkage and selection operator (LASSO); minimum redundancy maximum relevance (mRMR); and generalized linear model (GLM) as a machine-learning classifier. Independent predictive factors were determined to construct preoperative and postoperative radiomics nomograms by multivariate logistic regression analysis. The performances of the clinical model, radiomics algorithm, and radiomics nomogram in distinguishing GISTs with the *KIT* exon 11 mutation were evaluated by area under the curve (AUC) of the receiver operating characteristics.

RESULTS

Of 106 patients who underwent genetic analysis, 61 had the *KIT* exon 11 mutation. The combined radiomics algorithm was found to be the best prediction model for differentiating the expression status of the *KIT* exon 11 mutation (AUC = 0.836; 95% confidence interval [CI], 0.640–0.951) in the validation set. The clinical model, and preoperative and postoperative radiomics nomograms had AUCs of 0.606 (95% CI, 0.397–0.790), 0.715 (95% CI, 0.506–0.873), and 0.679 (95% CI, 0.468–0.847), respectively, with the validation set.

CONCLUSION

The radiomics algorithm could distinguish GISTs with the *KIT* exon 11 mutation based on CE-CT images and could potentially be used for selective genetic analysis to support the precision medicine of GISTs.

From the Department of Colorectal Surgery (B.L., H.L., Y.S., Z.Z., J.Z., J.Zhang ✉ Zhangjian@qduhospital.cn), the Affiliated Hospital of Qingdao University (Pingdu), and Department of Pathology (F.H.), Shandong, China; The Qingdao Grand International School (L.Z.), Shandong, China; Department of Radiology (S.Y.), the Shandong Provincial Hospital Affiliated to Shandong First Medical University, Shandong, China.

Received 18 June 2021; revision requested 12 July 2021; last revision received 10 October 2021; accepted 28 October 2021.

Published online 20 December 2021.

DOI 10.5152/dir.2021.21600

Gastrointestinal stromal tumors (GISTs) are the most commonly diagnosed subepithelial tumors of the gastrointestinal tract.^{1–3} However, GISTs respond poorly to chemotherapy and prognosis prediction is challenging because of their biological diversity and histological heterogeneity.² Mutations in the *KIT* gene, which encodes a tyrosine kinase, are known to lead to the development of GISTs. Besides *KIT*, mutations in other genes (e.g., *platelet-derived growth factor receptor alpha*, *PDGFRA*) have also been associated with GISTs.⁴

Most GISTs (75%–85%) have *KIT* mutations, 5%–7% have *PDGFRA* mutations, and 12%–15% have no detectable mutation in *KIT* or *PDGFRA*.^{1,4} The National Comprehensive Cancer Network (NCCN) guidelines highly recommend the genetic analysis of GISTs, because the expression status of specific regions of the *KIT* and *PDGFRA* gene sequences are correlated with a specific response to tyrosine kinase inhibitors (TKIs).² The *KIT* exon 11 mutation, which accounts for about 75% of *KIT* mutations in GISTs, is the most common imatinib-target mutation and GISTs with this mutation respond well to standard imatinib therapy.^{1,5–7} Because

You may cite this article as: Liu B, Liu H, Zhang L, et al. Value of contrast-enhanced CT based radiomic machine learning algorithm in differentiating gastrointestinal stromal tumors with *KIT* exon 11 mutation: a two-center study. *Diagn Interv Radiol.* 2022;28(1):29–38.

there are a fairly large number of patients who do not have the *KIT* exon 11 mutation, genetic analysis is required to define the wide variety of treatment effects.^{2,6,7} Therefore, before clinical treatment with TKIs, it is important to determine the expression status of the *KIT* exon 11 mutation. However, considering tolerance of the procedure and the heterogeneity of GISTs, conventional invasive biopsy or surgery to obtain specimens has many defects.^{2,8,9} Further, in our two centers, pathological specimens were obtained through biopsy and surgery, and routine pathological data such as mitotic count were analyzed. But patients still need to spend extra to get a genetic analysis of GISTs.^{10,11} Consequently, it is urgent to establish a noninvasive, repeatable, economical, and accurate pretreatment method to identify the expression status of the *KIT* exon 11 mutation.

Contrast-enhanced computed tomography (CE-CT) is a basic diagnostic method that is used to detect lesions and evaluate the treatment response of GISTs¹⁰⁻¹². Medical imaging has been playing an increasing key role in personalized precision medicine. Radiomics has been applied to oncology studies¹³ and has been widely used in diagnosis,¹⁴ prognostic evaluation,¹⁵ prediction of biological behaviors,¹⁶ and even genetic prediction.^{11,17} Previous studies have shown that gene mutation typing of GISTs is related to qualitative imaging features¹⁸⁻²⁰ and clinicopathological characteristics²¹⁻²⁴, so we included preoperative clinical and postoperative routine pathological data as predictive factors in this radiomics study. As

far as we know, there are still relatively few radiomics studies to predict the genotypes of GISTs.¹¹ Thus, the aim of this two-center study was to develop and validate a tri-phase CE-CT based radiomics model that can distinguish the patients with the *KIT* exon 11 mutation.

Methods

Study Design and Patient Population

In this retrospective study, we screened the patients with pathologically confirmed GISTs in the databases of these institutions from July 2008 to August 2019. Patients who fulfilled the following inclusion criteria were included in the study: a) patients with pathological specimens through biopsy or surgery for genetic analysis results; b) complete clinical characteristics; c) tri-phase CE-CT images before treatment (neoadjuvant therapy or surgery); and d) GIST size ≥ 2 cm and could be outlined in the CE-CT images for volume of interest segmentation.

According to these criteria, 106 patients who also underwent genetic analysis between August 2010 and August 2019 were included: 93 were from Affiliated Hospital of Qingdao University (Institution 1) and 13 were from Shandong Provincial Hospital Affiliated to Shandong First Medical University (Institution 2). Because the number of patients from institution 2 was small, their data could not be used as an external validation set alone. Therefore, the data of patients from both institutions were merged, then randomly allocated to training and validation sets in a 3:1 ratio. The number of patients with the *KIT* exon 11 mutation was 61, the number of patients without the *KIT* exon 11 mutation was 45. Among the 106 patients, 57 were male and 49 were female (mean age 59.5 ± 9.9 years).

Ethical statement

The authors are accountable for all aspects of the work in ensuring that questions related to the accuracy or integrity of any part of the work are appropriately investigated and resolved. This study was approved by both institutions' review boards (Approval number: QYFYWZLL25829) and the need for informed consent from patients was waived.

Tri-phase CE-CT image screening and volume of interest segmentation

All 106 patients had undergone CE-CT scanning with 16 or 64-detector spiral CT scanners (Siemens Somatom Definition, GE

Hispeed, GE Bright, or GE Optima 670). For all these measurements, the tube current was 200-240 mAs, the slice thickness was 5.0 mm, the tube voltage was 120-160 kV, and the injection rate was 3.5 mL/s, with intravenous injection of contrast (iopromide, 80 mL) and arterial, venous, and delayed phase with 30, 70, and 300 s delay, respectively.

ITK-SNAP (v3.6.0; www.itk-snap.org) was used for three-dimensional volume of interest (VOI) segmentation of the CE-CT images. VOI segmentation and feature extraction were performed in a blind manner by two radiologists. Radiologist 1, who had nine years' clinical experience, outlined the edge of the tumor on the tri-phase CE-CT images layer by layer and fused them into the VOIs. The same radiologist repeated the VOI segmentation and feature extraction after a two week wash out period. In addition, radiologist 2, who had 14 years' clinical experience, performed the VOI segmentation on the all CE-CT images and feature extraction once. Inter- and intraclass correlation coefficients (ICCs) were used to evaluate the reproducibility and stability of radiomics feature extraction to identify robust radiomics features. We randomly selected 30 cases of VOI segmentation performed by radiologist 1 and 2 for the ICCs. The interobserver ICC was derived from the first feature extraction by radiologist 1 and radiologist 2. The intraobserver ICC was derived from the feature extraction performed twice by radiologist 1. Generally, ICCs >0.75 are considered to indicate good reproducibility or reliability. In this study, to ensure highly accurate features were selected, an ICC >0.9 was used as a criterion for good robustness. The radiologists were blinded to the mutational analysis.

Image normalization and feature extraction

Some preprocessing was needed to improve texture recognition before feature extraction. First, the VOI was normalized by the $\mu \pm 3\sigma$ to highlight the differences between the classes.²⁵ Second, in order to reduce the computation time and improve the SNR of the texture results, the image was processed by using gray-level quantization (reducing the grayscale used to represent the image).²⁶ Finally, cubic interpolation was used to isotopically resample the VOIs to the in-plane resolution (0.5x0.5 mm) to ensure that the proportion and direction of the acquired three-dimensional features remain unchanged.²⁷

Main points

- Distinguishing the genetic phenotype of gastrointestinal stromal tumors (GISTs) is important for patients who receive targeted therapy with tyrosine kinase inhibitors.
- In the present study, we developed new arterial phase, venous phase, and delayed phase radiomics algorithms, a combined radiomics algorithm, preoperative and postoperative radiomics nomograms based on tri-phase contrast-enhanced CT.
- As a noninvasive tool, the combined radiomics algorithm facilitates the best prediction performance effectively.
- The combined radiomics algorithm achieves a satisfactory overall diagnostic accuracy for predicting the GISTs with *KIT* exon 11 mutation, showing an AUC of 0.836 (95% CI, 0.640-0.951) in the validation set.

The radiomics features of preprocessed CT images were extracted using commercial software (AnalysisKit v.: 1.0.3; GE Healthcare). The software can process the image texture features and quantitatively analyze the heterogeneity within the lesion.

For each phase CE-CT images, 4 types of features and 396 quantitative variables (10 Haralick feature, 42 Histogram features, 9 Morphological feature, 11 GLSZM features, 144 GLCM features and 180 RLM features) were extracted. The workflow process for

radiomics processing and analysis is presented in Figure 1.

Combat compensation method

The distinguishing features of the texture patterns were retained using the combat

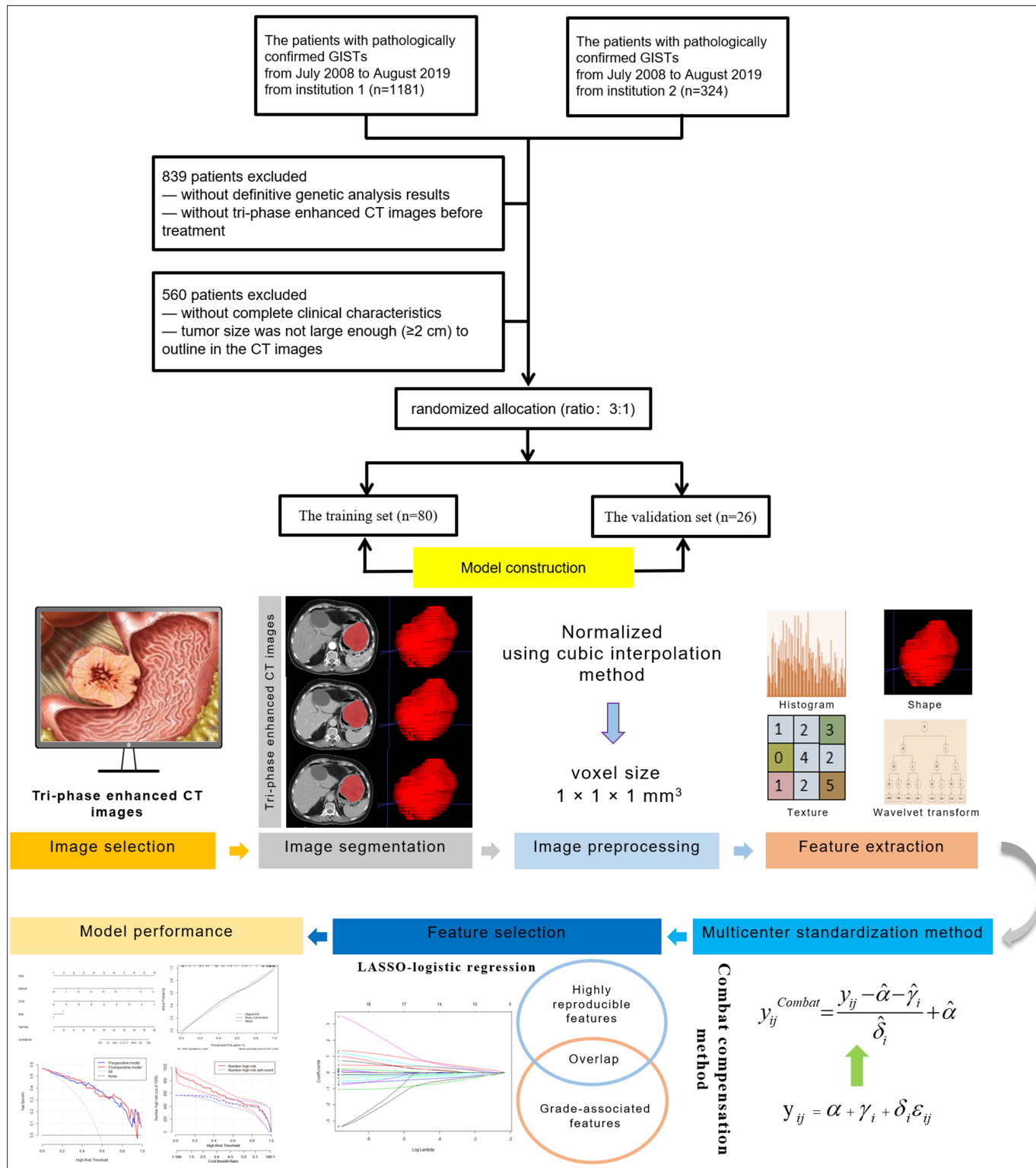


Figure 1. Workflow process for radiomics processing and analysis in this study.

compensation method,²⁸ while eliminating the influence of the scanner and the protocol. This method was helpful for multicenter radiomics analysis²⁹ and can be used for CE-CT images.

Clinical characteristics

The preoperative demographic and clinicopathologic data, including age, sex, and blood lab results (e.g., carcinoembryonic antigen (CEA), carbohydrate antigen 199 [CA199]), were collected for the 106 patients. Postoperative pathological data, including the location and size (maximum diameter) of the tumor, proteomics (e.g., expression statuses of tumor related proteins Ki-67, CD117, CD34, and DOG1), mitotic count, National Institutes of Health (NIH) risk stratification, growth pattern, and genetic phenotype were also collected.

For *KIT* and *PDGFRA* gene mutation analysis, a DNA extraction kit was used to extract DNA from pathological tissues, and primer design and PCR amplification was performed.

Clinical model, radiomics algorithm, and radiomics nomogram building

The relationship between clinical factors and the *KIT* exon 11 mutation was assessed by the univariate logistic regression. Then, the multivariate logistic model was used with the significant clinical features ($P < .05$) to develop the clinical model.

The feature extraction algorithm implemented in the R statistical software (v3.6.3; www.Rproject.org) was used to select features and generate each phase and tri-phase combined radiomics algorithm. During the algorithm construction, only the features with ICCs >0.9 were included. To select the most valuable predictive factors in the training set, we incorporated each phase and tri-phase CE-CT's the top 20 features of minimum redundancy maximum relevance (mRMR) into the least absolute shrinkage and selection operator method (LASSO) and fitted for regression of data. Generalized linear model (GLM) was used in this study, which is a machine-learning classifier and was trained with the training set using the 10-fold cross-validation approach. A radiomics algorithm was added with preoperative and postoperative clinical factors to build nomograms with multivariable logistic regression analysis. In the research design process, we considered that even if pathological specimens are obtained, routine genetic analysis of GIST has not been exten-

sively performed due to the high cost, so we decided to make full use of the preoperative and postoperative data to construct the preoperative and postoperative model.

Assessment and validation of the clinical model, radiomics algorithm, and radiomics nomogram

The effectiveness of the clinical model, radiomics algorithm, and radiomics nomogram in differentiating, calibration, and clinical value was verified with the validation set. The predictive capability was evaluated using the validation set by the receiver operating characteristic (ROC) curve, the area under the ROC curve (AUC), specificity, sensitivity, accuracy, and positive and negative predictive values. The calibration curves were used to assess the agreement between the predicted and actual results with the Hosmer–Lemeshow test.³⁰ The clinical applicability of the radiomics algorithm and preoperative and postoperative radiomics nomograms also was assessed with decision curve analysis by calculating the net benefit at different threshold probabilities.³¹

Statistical analysis

R statistical software (v3.6.3; www.Rproject.org) was used for all the statistical analyses. To select the clinical factors, Fisher's exact test or the chi-square test was used to compare the different groups of continuous variables in clinical characteristics. Mann-Whitney U test or independent t-test was used to evaluate the discrimination in clinical characteristics among different groups of continuous variables. Logistic regression was used to develop the clinical model and radiomics nomograms.

Results

Patients with GISTs were divided into two groups: those without the *KIT* exon 11 mutation and those with the *KIT* exon 11 mutation. The clinicopathologic and demographic data of these patients are summarized in Table 1. The expression status of CA724 and CD117 were significantly different between the two groups. No significant differences were found between any of the other clinical characteristics.

Because the ratio of the number of CD117 (-) ($n=0$) and (+) ($n=61$) in GISTs with the *KIT* 11 mutation is extremely asymmetric in the training set, we did not put this factor into the logistic regression in order not to produce meaningless results and errors. The

univariate logistic regression analysis of the clinical results showed that CA724 was significantly associated with GISTs with the *KIT* 11 mutation in the training set (Table 2). The multivariate logistic regression analysis of the clinical characteristics showed that CA724 ($P = .004$) and mitotic count ($P = .020$) were independent predictors of the *KIT* exon 11 mutation in GISTs (Table 2). We constructed preoperative and postoperative clinical models on the multivariate logistic regression results. The performances of the preoperative (CA724) and postoperative (CA724 and mitotic count) clinical models in distinguishing GISTs with the *KIT* exon 11 mutation are shown in Table 3. For the preoperative clinical model with the training and validation sets, the AUCs were 0.669 and 0.509 respectively; for the postoperative clinical model with the training and validation sets, the AUCs were 0.770 and 0.606 respectively.

Through the above tri-phase CE-CT data processing, we developed arterial phase (A-phase), venous phase (V-phase), delayed phase (D-phase), and tri-phase combined radiomics algorithms. Patients without the *KIT* exon 11 mutation generally had lower radiomics scores than patients with the *KIT* exon 11 mutation. The selected radiomics features of the A-phase, V-phase, D-phase, and combined radiomics algorithms are shown in Figure 2. The prediction efficiencies of the radiomics algorithms to distinguish GISTs with the *KIT* exon 11 mutation in the training and validation sets are shown in Table 4. The AUCs of the radiomics algorithms with the training and validation sets were 0.773 and 0.709, for the A-phase, 0.745 and 0.558 for the V-phase, 0.738 and 0.600 for the D-phase, and 0.826 and 0.836 for the combined radiomics algorithms, respectively (Figure 3). These results show that the predictive performance of the tri-phase combined radiomics algorithm was better than that of any of the single-phase algorithms.

The preoperative and postoperative clinical models and combined radiomics algorithm were incorporated into the multivariate logistic regression analysis to generate preoperative and postoperative radiomics nomograms, respectively (Figure 4a, 4d). The performances of preoperative and postoperative radiomics nomograms in distinguishing the patients with the *KIT* exon 11 mutation in the training and validation sets are shown in Table 3. For the preoperative radiomics nomogram with the training and validation sets, the AUCs were 0.913 and 0.715, respectively; for postoperative

Table 1. Clinicopathologic and demographic data

Clinical factors		<i>KIT</i> exon 11 mt (-) n=45	<i>KIT</i> exon 11 mt (+) n=61	<i>P</i>
Sex, n (%)	Male	22 (48.89)	35 (57.38)	0.386
	Female	23 (51.11)	26 (42.62)	
Age (years), median (range)		57 (47.50-66.50)	62 (55.00-66.00)	0.051
Growth pattern, n (%)	Endoluminal	12 (26.67)	20 (32.79)	0.238
	Exophytic	15 (35.56)	26 (42.62)	
	Mixed	18 (40.00)	15 (24.59)	
CEA (ng/mL), median (range)		1.76 (1.14-2.91)	2.00 (1.18-3.16)	0.623
CA199 (ng/mL), median (range)		10.61 (6.22-17.07)	8.64 (5.66-13.82)	0.215
CA125 (ng/mL), median (range)		10.06 (7.56-27.23)	9.06 (7.55-11.52)	0.144
CA724 (ng/mL), median (range)		4.40 (1.24-17.59)	1.49 (1.07-3.91)	0.006
Maximum diameter of tumor (cm), median (range)		5.00 (3.50-8.00)	5.00 (3.85-8.85)	0.468
Mitotic count (mitoses/50 hpf), n (%)	<5	31 (68.89)	32 (52.46)	0.089
	≥5	14 (31.11)	29 (47.54)	
Anatomic location, n (%)	Stomach	21 (46.67)	38 (62.30)	0.109
	Small bowel	18 (40.00)	20 (32.79)	
	Colorectum	2 (4.44)	2 (3.28)	
	Mesentery	4 (8.89)	1 (1.64)	
Ki-67 (%), median (range)		5 (3-11)	10 (5-20)	0.07
CD-117, n (%)	(-)	5 (11.11)	0 (0.00)	0.012
	(+)	40 (88.89)	61 (100.00)	
CD-34, n (%)	(-)	9 (20.00)	7 (11.48)	0.226
	(+)	36 (80.00)	54 (88.52)	
DOG-1, n (%)	(-)	4 (8.89)	1 (1.64)	0.16
	(+)	41 (91.11)	60 (98.36)	
NIH risk stratification (2008), n (%)	Very low	2 (4.44)	2 (3.28)	0.444
	Low	14 (31.11)	16 (26.23)	
	Intermediate	10 (22.22)	13 (21.31)	
	High	19 (42.22)	30 (49.18)	
Genetic phenotype, n (%)	<i>KIT</i> exon 9 mutation	24 (53.33)	-	-
	<i>KIT</i> exon 13 mutation	4 (8.89)	-	-
	<i>KIT</i> exon 14 mutation	3 (6.67)	-	-
	<i>KIT</i> exon 17 mutation	3 (6.67)	-	-
	<i>PDGFRA</i> exon 12 mutation	4 (8.89)	-	-
	<i>PDGFRA</i> exon 18 mutation	7 (15.56)	-	-

mt, mutation; (+), positive; (-), negative; CEA, carcinoembryonic antigen; CA199, carbohydrate antigen 199; CA125, carbohydrate antigen 125; CA724, carbohydrate antigen 724; NIH, National Institutes of Health.

radiomics nomogram with the training and validation sets, the AUCs were 0.919 and 0.679, respectively. The ROC curves for the training and validation sets were used to compare the prediction efficiencies of the combined radiomics algorithm and preoperative and postoperative radiomics nomograms (Figure 3). Interestingly, with

the training set, the preoperative and postoperative radiomics nomograms both had higher AUCs than the combined radiomics algorithm, whereas, with the validation set, the combined radiomics algorithm had a higher AUC than the three models.

The calibration curves of the combined radiomics algorithm (Figure 5c, 5d; $P = .781$

and .534) and preoperative (Figure 4b, 4c; $P = .838$ and .730) and postoperative (Figure 4e, 4f; $P = .899$ and .495) radiomics nomograms showed good calibration with the nonsignificant Hosmer–Lemeshow test statistic with the training and validation sets respectively. The decision curve analysis (DCA) showed that the combined radiomics

Table 2. Clinical factors of univariate and multivariate logistic regression analysis for KIT exon 11 mutation

Clinical characteristics	Univariate analysis			Multivariate analysis		
	OR	95% CI	P	OR	95% CI	P
Age (year)	1.03	0.99-1.06	0.18			
CA724 (ng/mL)	0.85	0.73-0.96	0.01	0.83	0.71-0.94	0.004
Mitotic count (mitoses/50 hpf)	2.33	1.36-3.29	0.08	4.24	3.02-5.45	0.02
Ki67(%)	1.04	1.00-1.07	0.09			

Mitotic count is included in the model as < 5 vs. ≥5 mitoses/50 hpf.
OR, odds ratio; CI, confidence interval.

Table 3. Prediction efficiencies of preoperative and postoperative clinical models and radiomics nomogram

		AUC	95% CI	Accuracy	Sensitivity	Specificity	PPV	NPV
Preoperative clinical model (CA724)	Training set	0.699	0.586-0.797	0.713	0.848	0.529	0.709	0.720
	Validation set	0.509	0.307-0.709	0.615	0.800	0.364	0.632	0.571
Postoperative clinical model (CA724 and mitotic count)	Training set	0.770	0.663-0.857	0.763	0.870	0.618	0.755	0.778
	Validation set	0.606	0.397-0.790	0.615	0.600	0.636	0.692	0.538
Preoperative radiomics nomogram	Training set	0.913	0.829-0.964	0.863	0.891	0.824	0.872	0.848
	Validation set	0.715	0.506-0.873	0.769	0.800	0.727	0.800	0.727
Postoperative radiomics nomogram	Training set	0.919	0.836-0.968	0.863	0.935	0.765	0.843	0.897
	Validation set	0.679	0.468-0.847	0.769	0.800	0.727	0.800	0.727

AUC, area under the receiver operating characteristic curve; CI, confidence interval; PPV, positive predictive value; NPV, negative predictive value.

Table 4. Prediction efficiencies of radiomics algorithm with the training and validation sets

		AUC	95% CI	Accuracy	Sensitivity	Specificity	PPV	NPV
A-phase radiomics algorithm	Training set	0.773	0.666-0.859	0.725	0.783	0.647	0.750	0.688
	Validation set	0.709	0.499-0.869	0.807	0.933	0.636	0.778	0.875
V-phase radiomics algorithm	Training set	0.745	0.635-0.836	0.687	0.565	0.853	0.839	0.592
	Validation set	0.558	0.351-0.750	0.731	0.867	0.546	0.722	0.750
D-phase radiomics algorithm	Training set	0.738	0.628-0.830	0.688	0.674	0.706	0.756	0.615
	Validation set	0.600	0.391-0.785	0.615	0.533	0.727	0.727	0.533
Tri-phase combined radiomics algorithm	Training set	0.826	0.725-0.902	0.763	0.696	0.853	0.865	0.674
	Validation set	0.836	0.640-0.951	0.808	0.800	0.818	0.857	0.750

AUC, area under the receiver operating characteristic curve; CI, confidence interval; PPV, positive predictive value; NPV, negative predictive value; A-phase, arterial phase; V-phase, venous phase; D-phase, delayed phase.

algorithm produced the highest overall net benefit compared with that of the preoperative or postoperative radiomics nomograms in predicting the *KIT* 11 mutation in the validation set across most of the range of reasonable threshold probabilities. However, the DCA found opposite results with the training set (Figure 5a, 5b).

Discussion

The specific *KIT* 11 mutation is associated with the clinical response to targeted therapy of GISTs.^{1,2,5} Selecting the targeted

therapies based on the GIST genotypes has made precision medicine for GISTs possible. Radiogenomics approaches decode image phenotypes using radiomics to predict the genotypes of tumors, and they have been applied successfully in precision medicine studies.^{11,17} In this retrospective two-center study, the aim was to develop a personalized radiomics method that could distinguish GISTs with the *KIT* exon 11 mutation by tri-phase CE-CT. In order to adapt to more diverse patients, flexibly use preoperative and postoperative data to develop clinical models, A-phase, V-phase, D-phase, and

tri-phase combined radiomics algorithms, and preoperative and postoperative radiomics nomograms. The results showed that the combined radiomics algorithm had a well-calibrated clinical benefit and the best ability to distinguish GISTs with the *KIT* exon 11 mutation in the validation set, which indicated that radiomics had accurate and reproducible value for predicting GISTs with the *KIT* exon 11 mutation genotype.

The clinical model was used to predict the biological behaviors of GISTs,³² and genotypes have been shown to be closely related to certain clinical characteristics.^{21,22,33}

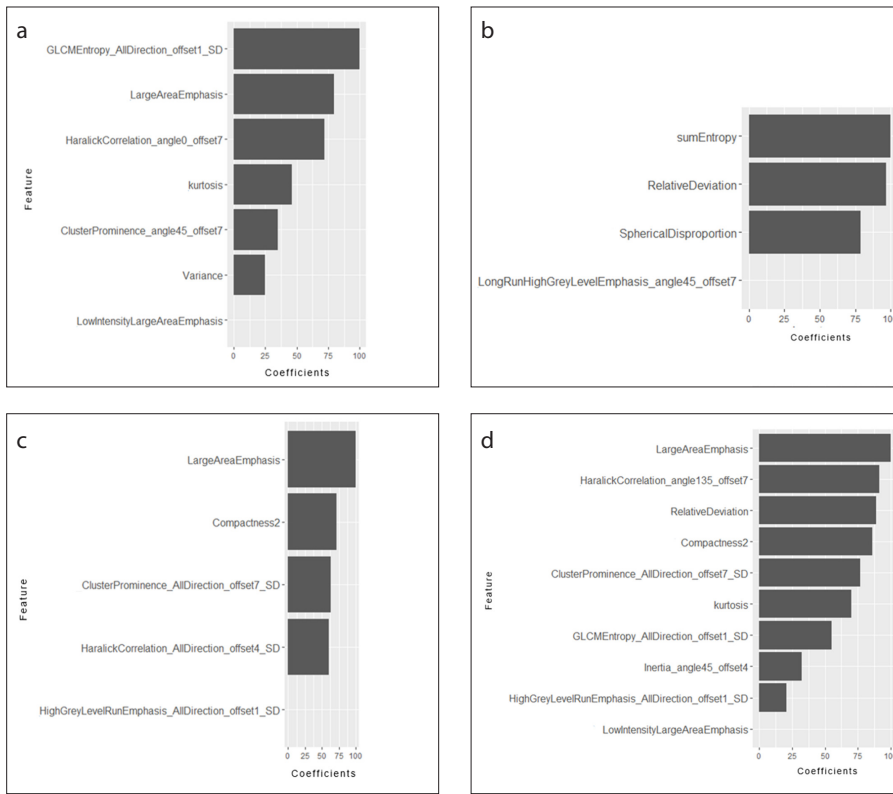


Figure 2. a–d. The selected radiomics features and their coefficients of the A-phase (a), V-phase (b), D-phase (c), and combined (d) radiomics algorithms. x-axis, coefficients of features with the LASSO logistic regression analysis; y-axis, features selected using the radiomics algorithms.

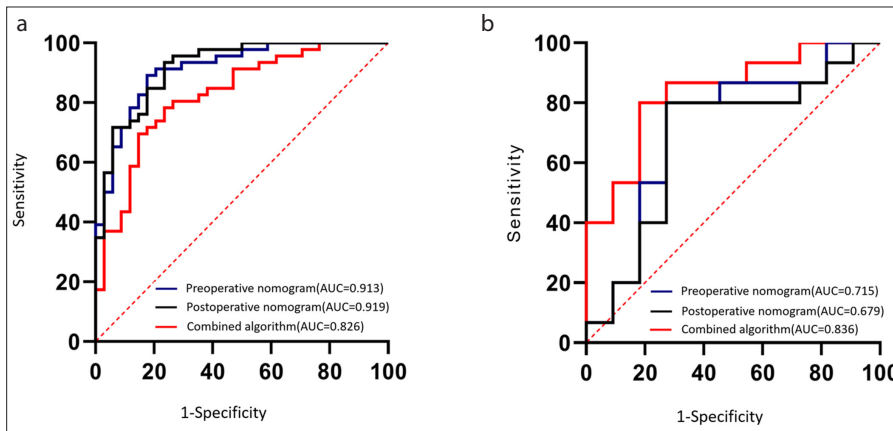


Figure 3. a, b. ROC curves for the combined radiomics algorithm, preoperative and postoperative radiomics nomograms with the training (a) and validation (b) sets.

However, the relationship between some clinical characteristics and the *KIT* 11 mutation remains controversial.^{21,23,24,33} Most of the previous studies showed that GISTs with the *KIT* exon 11 mutation usually had high percentages of mitotic count and/or poor prognosis.^{21,24,33} The relationship between CA724 and GIST genotypes has not been reported until now. We found that, in the training set, the mitotic count and CA724 were correlated with the GISTs with

the *KIT* exon 11 mutation. However, the preoperative and postoperative clinical models had relatively lower predictive effectiveness (AUC= 0.509 and 0.606) with the validation set than all the other models tested. This result indicated that the models based solely on clinical characteristics made only limited contributions to the discrimination performance. The roles of mitotic count and CA724 for differentiating the expression status of *KIT* exon 11 need further studies.

The extraction of high-dimensional features from medical images by radiomics has emerged as a promising approach for predicting the characteristics of tumors.^{11,13,15,17} Radiomics is more comprehensive than morphological visual analysis and can quantitatively reveal tumor heterogeneity. Various types of medical images can be analyzed to help with diagnosis and treatment and support traditional diagnostic methods.^{14,16,34,35} Previous studies have shown that gene mutation typing of GISTs is related to qualitative imaging features,^{18–20} the GISTs with the *KIT* exon 9 mutation were associated with a higher enhancement ratio and a tumor size larger than 10cm when compared with those with the *KIT* exon 11 mutation.¹⁸ Hyperenhancement of CT was more frequent in GISTs without *KIT* mutations compared to GISTs with *KIT* mutations.²⁰ Considering that GISTs of different genotypes may have heterogeneous blood supply and different CE-CT enhancement ratio.^{18,20} Using VOIs of all available slices extracted from tri-phase CE-CT images to construct a combined radiomics algorithm¹¹ can provide more information about a tumor,³⁶ and may have better clinical application value and generalizability in discriminating mutation.^{36–38} In the present study, we extracted more advanced radiomics features and used more data from two institutions compared with the CT texture analysis and single-center data in a previous study.¹¹ We also used various evaluation tools, better radiomics feature selection methods and machine-learning classifier to obtain the generalization and accuracy of the predictive model.

The radiomics algorithm was proven to be more effective than the clinical model. Next, we incorporated the clinical factors with the combined radiomics algorithm to build preoperative and postoperative radiomics nomograms. The AUC and DCA of the combined radiomics algorithm were compared with those of the preoperative and postoperative radiomics nomograms. The results showed that the combined radiomics algorithm had better predictive effectiveness and clinical applicability with the validation set than the radiomics nomograms, which indicated that the radiomics algorithm reflected molecular-level pathology better than the clinical factors and confirmed the enormous potential of the radiomics algorithm to distinguish GISTs with the *KIT* 11 mutation.

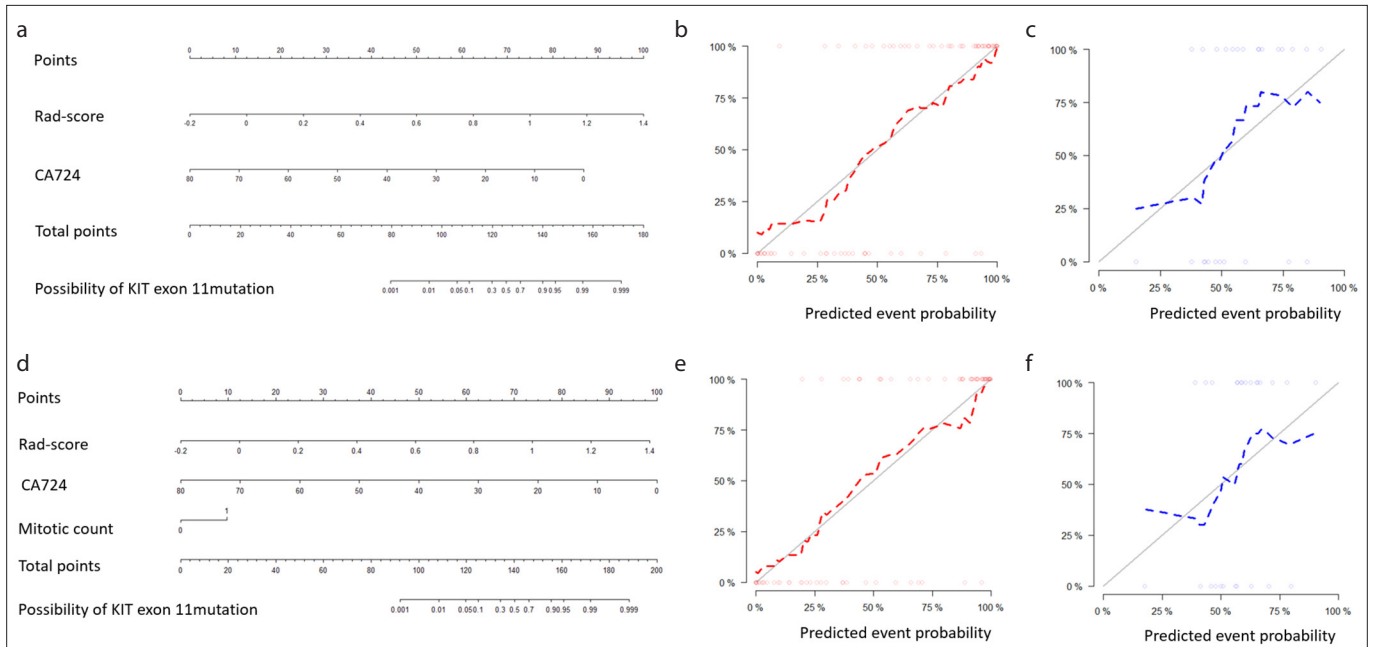


Figure 4. a–f. Preoperative radiomics nomogram (a) for predicting the *KIT* exon 11 mutation. Calibration curves of the preoperative radiomics nomogram with the training (b) and validation (c) sets. Postoperative radiomics nomogram (d) for predicting the *KIT* exon 11 mutation. Calibration curves of postoperative radiomics nomogram with the training (e) and validation (f) sets.

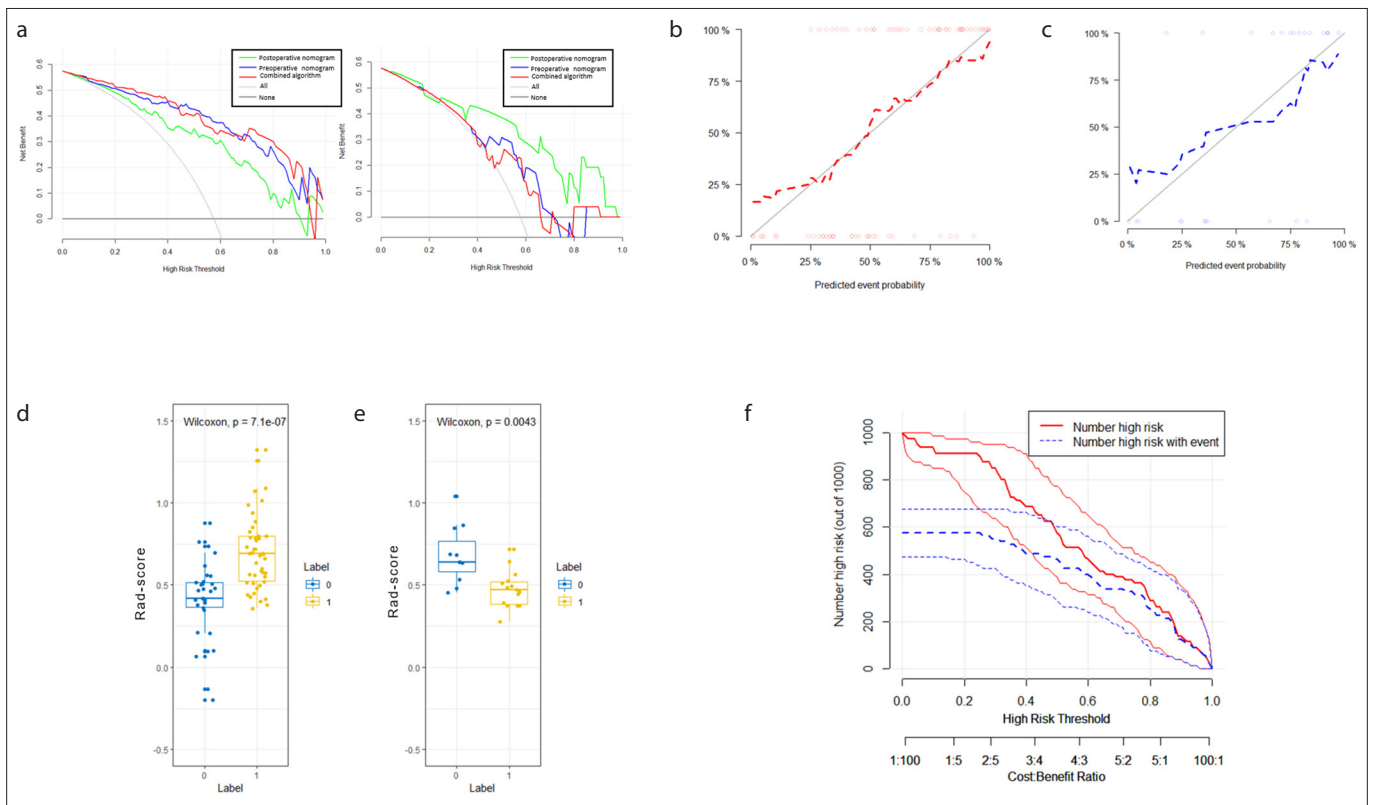


Figure 5. a–f. Decision curve analysis (DCA) for the combined radiomics algorithm, and preoperative and postoperative radiomics nomograms with the training (a) and validation (b) sets. The combined radiomics algorithm had the highest net benefit when the threshold probability was between 0.3 and 1 in the validation set, compared with the simple strategies of no patients (*horizontal black line*) or all patients (*grey line*) and other methods. Calibration curves of combined radiomics algorithm with the training (c) and validation (d) sets. Validation of radiomics scores (rad-scores) (e), with *blue* and *yellow* showing the actual classification. Low degree of mix of *blue* and *yellow* indicates good predictive ability of the rad-score; complete separation of *blue* and *yellow* indicates that the rad-score can be well classified. Clinical impact curves (f) of the combined radiomics algorithm. Number high risk with event (*blue curve*) is the number of true positives at each threshold probability; number high risk (*red curve*) indicates the number of patients classified as positive by the algorithm at each threshold probability.

To prevent overfitting, the mRMR and LASSO regression methods were applied to the extracted features. For feature selection, we used mRMR, which is a new feature screening method,³⁴ to screen radiomics features that have the fewest redundancies and most credible coefficients. LASSO is a feature screening method for selecting the predominant features of both ridge regression and subset screening.³⁹ We used GLM as a machine-learning classifier because it was reported to produce the best screening performance among the 11 machine-learning methods that were tested.³⁵ With application of the excellent feature selection methods and machine-learning classifier, the combined radiomics algorithm satisfactorily distinguished GISTs with and without the *KIT* exon 11 mutation.

The development of targeted therapy and genetic analysis have made the precision medicine feasible for GISTs.^{5,11,22,33} The most common imatinib-target mutation is the *KIT* exon 11 mutation, and patients with this mutation can benefit from standard imatinib therapy.^{2,4,5,10} The relatively rare patients without the *KIT* exon 11 mutation require further genetic analysis to identify multiple effects of different treatments.^{1,2,4-6} The combined radiomics algorithm developed in this study may provide a supplement to biopsies, which also have many challenges,^{2,8,10} to distinguish GISTs with the *KIT* exon 11 mutation noninvasively. For patients who were evaluated as the *KIT* exon 11 mutation of high probability with the combined radiomics algorithm, clinicians could recommend the standard imatinib therapy.

Our study has several limitations. First, all data were collected retrospectively and limited to Chinese patients, so selection bias was inevitable. Second, although the data were from two centers, the proportion of samples that had been performed genetic analysis was small, possibly because of cost considerations, which highlights the need for and significance of radiomics analysis. These findings need to be validated in international, larger multi-institutional studies. Third, only CE-CT images (slice thickness of 5.0 mm) were analyzed in this study. Whether radiomics could achieve a better performance on different slice thickness of CE-CT is worth further investigation. Fourth, the hand-crafted feature requires time-consuming tumor boundary segmentation, deep learning radiomics could accurately

and automatically detect and segment and achieve excellent performances.¹⁷ Lastly, this study includes radiomic features from the tri-phase CE-CT. Due to difference in protocols between different institutions, the delayed phase is not always performed in GIST's staging, which may limit the general applicability of the models.

In conclusion, we developed and validated several predictive models that could noninvasively distinguish GISTs with *KIT* exon 11 mutation based on tri-phase CE-CT images. The combined radiomics algorithm performed better than the other predictive models, which confirmed it as a potential predictor to supplement conventional approaches for selective genetic analysis and to support the clinical decision about imatinib therapy in the precision medicine of GISTs.

Acknowledgments

The authors thank the editors of Liwen Bianji for language editing.

Financial disclosure

This work was supported by National Natural Science Foundation of China (grant number 81770631).

Conflict of interest disclosure

The authors declared no conflicts of interest.

References

1. Heinrich MC, Corless CL, Demetri GD, et al. Kinase mutations and imatinib response in patients with metastatic gastrointestinal stromal tumor. *J Clin Oncol*. 2003;21(23):4342-4349. [\[Crossref\]](#)
2. Randall RL, Benjamin RS, Boles S, et al. Soft Tissue Sarcoma, Version 1.2018, NCCN Clinical Practice Guidelines in Oncology. *J Natl Compr Canc Netw*. 2018;16(5):536-563. [\[Crossref\]](#)
3. Edmonson JH, Marks RS, Buckner JC, Mahoney MR. Contrast of response to dacarbazine, mitomycin, doxorubicin, and cisplatin (DMAP) plus GM-CSF between patients with advanced malignant gastrointestinal stromal tumors and patients with other advanced leiomyosarcomas. *Cancer Invest*. 2002;20(5-6):605-612. [\[Crossref\]](#)
4. Oppelt PJ, Hirbe AC, Van Tine BA. Gastrointestinal stromal tumors (GISTs): point mutations matter in management, a review. *J Gastrointest Oncol*. 2017;8(3):466-473. [\[Crossref\]](#)
5. Heinrich MC, Owzar K, Corless CL, et al. Correlation of kinase genotype and clinical outcome in the North American Intergroup Phase III Trial of imatinib mesylate for treatment of advanced gastrointestinal stromal tumor: CALGB 150105 Study by Cancer and Leukemia Group B and Southwest Oncology Group. *J Clin Oncol*. 2008;26(33):5360-5367. [\[Crossref\]](#)
6. Chen P, Zong L, Zhao W, Shi L. Efficacy evaluation of imatinib treatment in patients with gastrointestinal stromal tumors: a meta-analysis. *World J Gastroenterol*. 2010;16(33):4227-4232. [\[Crossref\]](#)

7. Corless CL, Ballman KV, Antonescu CR, et al. Pathologic and molecular features correlate with long-term outcome after adjuvant therapy of resected primary GI stromal tumor: the ACOSOG Z9001 trial. *J Clin Oncol*. 2014;32(15):1563-1570. [\[Crossref\]](#)
8. Kim GH, Ahn JY, Gong CS, et al. Efficacy of Endoscopic Ultrasound-Guided Fine-Needle Biopsy in Gastric Subepithelial Tumors Located in the Cardia. *Dig Dis Sci*. 2019;65:583-590. [\[Crossref\]](#)
9. Chen T, Xu L, Dong X, et al. The roles of CT and EUS in the preoperative evaluation of gastric gastrointestinal stromal tumors larger than 2 cm. *Eur Radiol*. 2019;29(5):2481-2489. [\[Crossref\]](#)
10. Li J, Ye Y, Wang J, et al. Chinese consensus guidelines for diagnosis and management of gastrointestinal stromal tumor. *Chin J Cancer Res*. 2017;29(4):281-293. [\[Crossref\]](#)
11. Xu F, Ma X, Wang Y, et al. CT texture analysis can be a potential tool to differentiate gastrointestinal stromal tumors without KIT exon 11 mutation. *Eur J Radiol*. 2018;107:90-97. [\[Crossref\]](#)
12. Choi H. Response evaluation of gastrointestinal stromal tumors. *Oncologist*. 2008;13:4-7. [\[Crossref\]](#)
13. Lambin P, Leijenaar RTH, Deist TM, et al. Radiomics: the bridge between medical imaging and personalized medicine. *Nat Rev Clin Oncol*. 2017;14(12):749-762. [\[Crossref\]](#)
14. Nie P, Yang G, Wang Z, et al. A CT-based radiomics nomogram for differentiation of renal angiomyolipoma without visible fat from homogeneous clear cell renal cell carcinoma. *Eur Radiol*. 2020;30(2):1274-1284. [\[Crossref\]](#)
15. Liu S, He J, Liu S, et al. Radiomics analysis using contrast-enhanced CT for preoperative prediction of occult peritoneal metastasis in advanced gastric cancer. *Eur Radiol*. 2020;30(1):239-246. [\[Crossref\]](#)
16. Nie P, Yang G, Wang N, et al. Additional value of metabolic parameters to PET/CT-based radiomics nomogram in predicting lymphovascular invasion and outcome in lung adenocarcinoma. *Eur J Nucl Med Mol Imaging*. 2020:217-230. [\[Crossref\]](#)
17. Zhao W, Yang J, Ni B, et al. Toward automatic prediction of EGFR mutation status in pulmonary adenocarcinoma with 3D deep learning. *Cancer Med*. 2019;8(7):3532-3543. [\[Crossref\]](#)
18. Yin YQ, Liu CJ, Zhang B, Wen Y, Yin Y. Association between CT imaging features and KIT mutations in small intestinal gastrointestinal stromal tumors. *Sci Rep*. 2019;9(1):7257. [\[Crossref\]](#)
19. Tateishi U, Miyake M, Maeda T, Arai Y, Seki K, Hasegawa T. CT and MRI findings in KIT-weak or KIT-negative atypical gastrointestinal stromal tumors. *Eur Radiol*. 2006;16(7):1537-1543. [\[Crossref\]](#)
20. Cannella R, Tabone E, Porrello G, et al. Assessment of morphological CT imaging features for the prediction of risk stratification, mutations, and prognosis of gastrointestinal stromal tumors. *Eur Radiol*. 2021:1-11. [\[Crossref\]](#)
21. Baskin Y, Kocal GC, Kucukzeybek BB, et al. PDGFRA and KIT Mutation Status and Its Association With Clinicopathological Properties, Including DOG1. *Oncol Res*. 2016;24(1):41-53. [\[Crossref\]](#)

22. Wozniak A, Rutkowski P, Piskorz A, et al. Prognostic value of KIT/PDGFRA mutations in gastrointestinal stromal tumours (GIST): Polish Clinical GIST Registry experience. *Ann Oncol*. 2012;23(2):353-360. [\[Crossref\]](#)
23. Vitiello GA, Bowler TG, Liu M, et al. Differential immune profiles distinguish the mutational subtypes of gastrointestinal stromal tumor. *J Clin Invest*. 2019;129(5):1863-1877. [\[Crossref\]](#)
24. Capelli L, Petracci E, Quagliuolo V, et al. Gastric GISTs: Analysis of c-Kit, PDGFRA and BRAF mutations in relation to prognosis and clinical pathological characteristics of patients - A GIRCG study. *Eur J Surg Oncol*. 2016;42(8):1206-1214. [\[Crossref\]](#)
25. Collewet G, Strzelecki M, Mariette F. Influence of MRI acquisition protocols and image intensity normalization methods on texture classification. *Magn Reson Imaging*. 2004;22(1):81-91. [\[Crossref\]](#)
26. Gibbs P, Turnbull LW. Textural analysis of contrast-enhanced MR images of the breast. *Magn Reson Med*. 2003;50(1):92-98. [\[Crossref\]](#)
27. Depeursinge A, Foncubierta RA, Van DVD, Müller H. Three-dimensional solid texture analysis in biomedical imaging: review and opportunities. *Med Image Anal*. 2014;18(1):176-196. [\[Crossref\]](#)
28. Orlhac F, Frouin F, Nioche C, Ayache N, Buvat I. Validation of A Method to Compensate Multicenter Effects Affecting CT Radiomics. *Radiol*. 2019;291(1):53-59. [\[Crossref\]](#)
29. Fortin JP, Cullen N, Sheline YI, et al. Harmonization of cortical thickness measurements across scanners and sites. *NeuroImage*. 2018;167:104-120. [\[Crossref\]](#)
30. Iasonos A, Schrag D, Raj GV, Panageas K. How to build and interpret a nomogram for cancer prognosis. *J Clin Oncol*. 2008;26(8):1364-13670. [\[Crossref\]](#)
31. Vickers AJ, Elkin EB. Decision curve analysis: a novel method for evaluating prediction models. *Med Decis Making: Int J Soc Med Decis Making*. 2006;26(6):565-574. [\[Crossref\]](#)
32. Gold JS, Gonen M, Gutierrez A, et al. Development and validation of a prognostic nomogram for recurrence-free survival after complete surgical resection of localised primary gastrointestinal stromal tumour: a retrospective analysis. *Lancet Oncol*. 2009;10(11):1045-1052. [\[Crossref\]](#)
33. Quek R, Farid M, Kanjanapan Y, et al. Prognostic significance of KIT exon 11 deletion mutation in intermediate-risk gastrointestinal stromal tumor. *Asia Pac J Clin Oncol*. 2017;13(3):115-124. [\[Crossref\]](#)
34. Lu W, Zhong L, Dong D, et al. Radiomic analysis for preoperative prediction of cervical lymph node metastasis in patients with papillary thyroid carcinoma. *Eur J Radiol*. 2019;118:231-238. [\[Crossref\]](#)
35. Parmar C, Grossmann P, Rietveld D, Rietbergen MM, Lambin P, Aerts HJ. Radiomic Machine-Learning Classifiers for Prognostic Biomarkers of Head and Neck Cancer. *Front Oncol*. 2015;5:272. [\[Crossref\]](#)
36. Ng F, Kozarski R, Ganeshan B, Goh V. Assessment of tumor heterogeneity by CT texture analysis: can the largest cross-sectional area be used as an alternative to whole tumor analysis? *Eur J Radiol*. 2013;82(2):342-348. [\[Crossref\]](#)
37. Zhou C, Duan X, Zhang X, Hu H, Wang D, Shen J. Predictive features of CT for risk stratifications in patients with primary gastrointestinal stromal tumour. *Eur Radiol*. 2016;26(9):3086-3093. [\[Crossref\]](#)
38. Jiang Z, Zhang J, Li Z, Liu Y, Wang D, Han G. A meta-analysis of prognostic value of KIT mutation status in gastrointestinal stromal tumors. *Oncotargets Ther*. 2016;9:3387-3398. [\[Crossref\]](#)
39. Gui J, Li H. Penalized Cox regression analysis in the high-dimensional and low-sample size settings, with applications to microarray gene expression data. *Bioinformatics*. 2005;21(13):3001-3008. [\[Crossref\]](#)